Optical and Quantum Electronics (2018)50:393
https://doi.org/10.1007/s11082-018-1661-3

Adiabatic transfer of surface plasmons in non-Hermitian graphene waveguides

Shaolin Ke[1] · Dong Zhao[2,3] · Qingjie Liu[2] · Weiwei Liu[2]

Received: 16 April 2018 / Accepted: 11 October 2018

Abstract
We investigate the energy transfer of surface plasmon polaritons (SPPs) based on adiabatic passage in a non-Hermitian waveguide composed of three coupled graphene sheets. The SPPs can completely transfer between two outer waveguides via the adiabatic dark mode as the waveguides are lossless and the coupling length is long enough. However, the loss of graphene can lead to breakdown of adiabatic transfer schemes. By utilizing the coupled mode theory, we propose three approaches to cancel the nonadiabatic coupling by adding certain gain or loss in respect waveguides. Moreover, the coupling length of waveguide is remarkably decreased. The study may find interesting application in optical switches on a deep-subwavelength scale.

Keywords Waveguides · Subwavelength structures · Plasmonics

1 Introduction

Graphene, which can support surface plasmon polaritons (SPPs) in the THz and far-infrared frequencies, recently has attracted great attention in manipulating light propagation to conquer the limitation of diffraction (Bao and Loh 2012; Konstantatos et al. 2012; Wang et al. 2017a, b, 2018a; Gramotnev and Bozhevolnyi 2010; Gan et al. 2017; Sun et al. 2016; Deng et al. 2015). SPPs in graphene experience stronger field confinement when comparing with metal thanks to its unique electrical and optical properties (Bao and Loh 2012). The surface conductivity of graphene can be flexibly tuned by electrostatic and chemical doping, which can be utilized to design active devices (Deng et al. 2016). The high carrier mobility in graphene makes it suitable for ultra-fast switching (Ni et al. 2016; He et al. 2018a). The nonlinearity of graphene also can benefit to the design of all optical switches (Wang et al. 2017c; Kou et al. 2013; Qin et al.

✉ Weiwei Liu
lwhust@hust.edu.cn

[1] Laboratory of Optical Information Technology, Wuhan Institute of Technology, Wuhan 430205, China

[2] School of Physics, Huazhong University of Science and Technology, Wuhan 430074, China

[3] School of Electronics Information and Engineering, Hubei University of Science and Technology, Xianning 437100, China

Published online: 17 October 2018

2018; Liu et al. 2018a; Zhao et al. 2017). Many plasmonic circuits based on graphene, such as ring resonators (Huang et al. 2014) and mode convertors (Ke et al. 2017), are proposed to operate on a deep-subwavelength scale. When the surface conductivity of graphene undergoes spatial–temporal modulation, the wave propagation can become non-reciprocal (Qin et al. 2016). For the forward direction, light experiences mode conversion between different frequencies. At the same time, the modulation has no effect on the light propagation in the backward direction (Sounas and Alù 2017).

Recently, the optical waveguides based on adiabatic theorem are also utilized in designing integrated photonics circuits in both Hermitian and non-Hermitian systems (Ke et al. 2016, 2017; Vitanov et al. 2017; Liu et al. 2018b; Ke et al. 2018c; Paspalakis 2006; Torosov et al. 2014; Graefe et al. 2013; Sharaf et al. 2018; Wu et al. 2016; Ibáñez and Muga 2014; Li et al. 2017; Milburn et al. 2015). One important scheme is the stimulated Raman adiabatic passage (STIRAP), which is studied in a three weekly coupled waveguides (Vitanov et al. 2017; Paspalakis 2006). The three-waveguide coupler supports one dark eigenmode as the energy dominates at outer two waveguides and no energy resides at center waveguide. The adiabatic theorem states that the system remains in its instantaneous eigenmodes if the parameters vary slowly enough (Milburn et al. 2015; Ke et al. 2016). By slightly altering the coupling strength between adjacent waveguides, the system remains at the dark mode during the propagation. As a result, light can completely transfer between outer two waveguides and the center waveguide has no energy. Efficient optical switches can be realized based on the STIRAP, which are robust against the propagation loss of center waveguide and perturbation of waveguide parameters including the interlayer spacing and refractive index. Moreover, the bandwidth of operating wavelength is increased as well (Vitanov et al. 2017). The STIRAP has been investigated in linear and nonlinear dielectric waveguides (Vitanov et al. 2017; Paspalakis 2006) and also plasmonic waveguides composed of densely packed metallic waveguides (Mrejen et al. 2015). The fractional STIRAP is also experimentally demonstrated in Dreisow et al. (2009) where the couplings terminate simultaneously with equal values of their strength. In this way, the light is split equally between two outer waveguides, which are helpful to design robust waveguide splitters.

In this work, we investigate the STIRAP in a waveguide composed of three spatially separated graphene sheets. The SPPs can completely transfer between outer two sheets when loss of graphene is not considered. Actually, graphene is lossy due to the finite relaxation time of electrons. One has also utilized optical pumping to realize nonlinear conversion and carrier injection to compensate the loss and realize optical gain in graphene (Boubanga-Tombet et al. 2012; Ryzhii et al. 2011; Li et al. 2012; Hong et al. 2017, 2018; De Leon and Berini 2010). The nonlinear phenomena have attracted a lot attention and find great application in recent years (Ma et al. 2018; Tan et al. 2018; He et al. 2017; Yuan et al. 2017; Wang et al. 2018b; Chen et al. 2018; Yuan et al. 2018; Li et al. 2018; He et al. 2018b; Lan et al. 2017; Liu et al. 2018c; He et al. 2018c). The system associated with gain and loss is non-Hermitian, which provides new possibility to modulate the flow of light (Makris et al. 2008; Ke et al. 2018a; Zhao et al. 2018). In general, the propagation constants of non-Hermitian waveguides are complex-valued. Specially, the non-Hermitian systems may possess real propagation constants when the parity-time (PT) symmetry is sustained (Zhao et al. 2018). PT symmetric systems are invariant under parity and time-reversal operations. The condition is satisfied when the refractive index along the transverse direction is $n(x)=n^*(-x)$ (Makris et al. 2008). Loss induced amplification (Lin et al. 2016a), efficient field tailoring (Lin et al. 2016b), enhanced sensing (Chen and Jung 2016), and strong absorption (Ke et al. 2018b) are proposed in the realm of graphene plasmonics

by taking advantage of the non-Hermitivity. Here, we study the influence of gain and loss on the STIRAP in graphene waveguides. The adiabatic transfer breaks down when the intrinsic loss of graphene is considered. By utilizing the coupled mode theory, we show the suitably distributed gain and loss can effectively suppress the nonadiabatic coupling and increase the coupling length of the waveguides can be effectively decreased.

2 Adiabatic passage

Figure 1 schematically depicts the structure under consideration, which consists of three graphene sheets embedded in the host dielectric with a permittivity ε_d. The host dielectric is assumed to be air for simplicity with $\varepsilon_d=1$. The three graphene sheets possess different surface conductivities labeled as σ_1, σ_2, and σ_3, which relate to the incident wavelength λ, chemical potential μ, relaxation time τ, and temperature T. The surface conductivity can be figured out by using the Kubo formula (Bao and Loh 2012). Here the room temperature is assumed as $T=300$ K, incident wavelength is $\lambda=10$ μm, and the chemical potential of graphene is fixed at $\mu=0.15$ eV. We first consider the lossless cases and the relaxation time of graphene are assumed to be infinite. The influences of loss will be discussed later. The interlayer spacing is denoted as d_1 and d_2, respectively. The center graphene sheet is obliquely placed such that the spacing between adjacent waveguides is varied. The spacing satisfies the relation $d_1=d_0+(d-2d_0)z/L$ and $d_2=d-d_1$, where d_0 is the initial value of spacing d_1 at $z=0$, L is the total length of the waveguides, and d denotes the total spacing between two outer waveguides. The parameters are chosen as $d_0=80$ nm, $d=220$ nm, and $L=50$ μm. The SPPs of TM polarization are considered, which propagate along z direction. When the SPPs are launched from the right waveguides, the energy adiabatically transfers to left waveguide and the output energy almost completely resides at the left waveguide. The energy transfer can be understood from the coupled mode theory.

The waveguides are weekly coupled as the interlayer spacing is larger than the plasmonic thickness. The time vary term is chosen as $\exp(-j\omega t)$ throughout the study. Then, the amplitudes of SPPs in respective waveguides A_1, A_2, and A_3 evolve according to the coupled mode theory $-i\mathrm{d}\mathbf{A}/\mathrm{d}z=\mathbf{HA}$ with $\mathbf{A}=(A_1, A_2, A_3)^{\mathrm{T}}$ and $\mathbf{H}$ given by

$$H=\begin{pmatrix}\beta_0 & c_1 & 0\\ c_1 & \beta_0 & c_2\\ 0 & c_2 & \beta_0\end{pmatrix}. \tag{1}$$

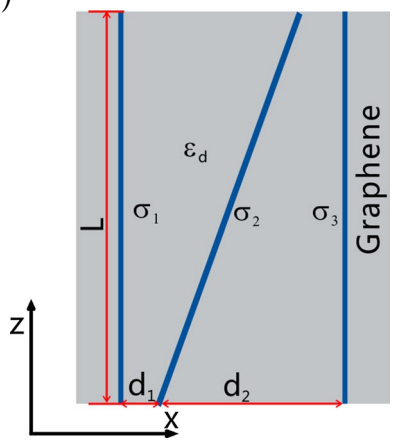

Fig. 1 Schematic of adiabatic three coupled graphene waveguides

β_0 denotes the propagation constant of SPPs in the single graphene sheet, c_1 and c_2 represent the coupling coefficients. The eigenvalues of Eq. (1) is derived as

$$\beta_1 = \beta_0, \quad \beta_{2,3} = \beta_0 \pm \sqrt{c_1^2 + c_2^2} \tag{2}$$

The corresponding eigenstates read as

$$\mathbf{A}_1 = \begin{pmatrix} \cos\theta \\ 0 \\ -\sin\theta \end{pmatrix}, \quad \mathbf{A}_{2,3} = \frac{1}{\sqrt{2}} \begin{pmatrix} \sin\theta \\ \pm 1 \\ \cos\theta \end{pmatrix} \tag{3}$$

with $\tan\theta = c_1/c_2$. In the waveguides, the propagation constants and mode profiles are determined by the eigenvalues and eigenstates, respectively. Mode $\mathbf{A}_1$ is referred as dark mode as no energy resides at center waveguide for different coupling strength, which can be utilized to transfer SPPs according to adiabatic theorem. When θ changes from $\pi/2 (c_1 >> c_2)$ to $0 (c_1 << c_2)$, the mode $\mathbf{A}_1$ alters form $(0, 0, -1)^{\mathrm{T}}$ to $(1, 0, 0)^{\mathrm{T}}$. According adiabatic theorem, the system remains in its instantaneous eigenstates if the coupling strength varies slowly enough along the propagation direction. Therefore, the SPPs can gradually transfer from right waveguides to the left one. Moreover, the center waveguide will remain dark throughout the process.

Figure 2 show the numerical results of STIRAP in graphene waveguides. In Fig. 2a, we plot the instantaneous eigenvalues along the propagation direction. The instantaneous eigenvalues are position dependent propagation constants. At a certain distance, the waveguide experiences different spacing d_1 and d_2 and thus different propagation constants $\beta(d_1, d_2)$, which can be calculated using transfer matrix method (TMM). Their following mode profiles are called as instantaneous eigenstates. There are three SPP modes supported in the system. The different colors of blue, red, and green represent modes $\mathbf{A}_1$, $\mathbf{A}_2$, and $\mathbf{A}_3$, respectively. The propagation constants of dark mode $\mathbf{A}_1$ remain unchanged at different positions and equal to $\beta_0 = 43.4\ \mu\mathrm{m}^{-1}$. The propagation constants of other two modes vary with increasing distance z, but they have same value at two waveguide terminals because the spacing d_1 and d_2 exchanges with each other. Figure 2b presents the mode profiles ($|H_y|^2$) of the dart mode $\mathbf{A}_1$ at different positions. The field intensity is normalized by the total energy at each position z. The coupling strength exponentially decays with increasing interlay spacing. At the starting position ($z = 0$), we have $\theta \approx \pi/2$ as $d_1 \ll d_2$. Therefore, the energy mainly concentrates at right waveguide. At the end of the waveguide, we have

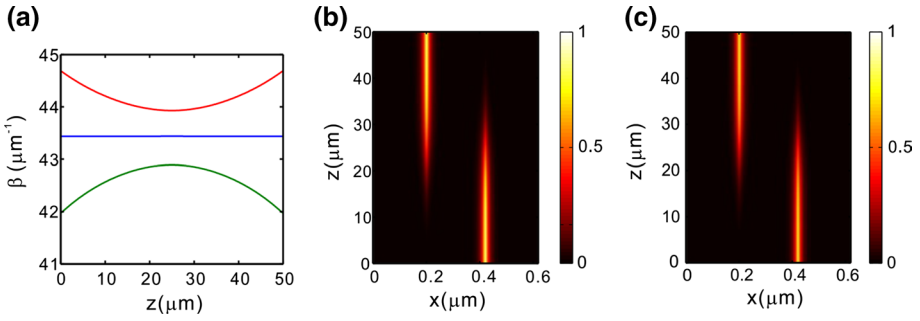

Fig. 2 The adiabatic energy transfer in lossless graphene waveguide. **a**, **b** are the instantaneous eigenvalues and eigenstates, respectively. **c** The propagation of SPPs as the right waveguide is excited

$\theta \approx 0$ as $d_1 \gg d_2$ and the energy is mainly confined at the left waveguide. There is always no energy residing at center waveguide for different positions. The results are accommodated with the theoretical indication. According to adiabatic theory, the system remains in its instantaneous eigenstates if the parameters vary slowly enough. Therefore, the propagation of SPPs will follow the prediction of instantaneous eigenstates shown in Fig. 2b. Figure 2c show the simulated wave propagation as the SPPs are injected through the right graphene sheet, which corresponds to the initial states being dark mode $\mathbf{A}_1 = (0, 0, 1)^{\mathrm{T}}$. The wave evolutions are simulated by using the finite element method (FEM) performed by Comsol Multiphysics. Graphene is modeled by employing the surface current boundary condition (Huang et al. 2017). The domain has been discretized less than 1/12 of SPP wavelength. One can see the SPPs gradually transfer from right waveguide to the left one with center waveguide been dark during the propagation. Therefore, efficient energy transfer can emerge by using the dark mode and the adiabatic theorem. The process is robust against the perturbation as the transfer efficiency is determined by the ratio of coupling strength c_1/c_2 at the output and irrelevant with local detail of waveguide parameters.

3 Breakdown of adiabatic transfer

3.1 Influence of propagation distance

The adiabatic evolution requires that the system parameters should vary slowly. In this scheme, the propagation distance determines the change speed of coupling strength. The adiabatic transfer will break down for short propagation distance L. Figure 3a shows the propagation of SPPs as $L = 10$ μm. Other parameters keep unchanged. One can see the center waveguide no longer remains dark during the propagation. The energy resides at both left and right waveguides at the output of graphene waveguide. This is because the SPPs no longer keep in the instantaneous eigenstates of dark mode ($\mathbf{A}_1$) and transfer to other two modes ($\mathbf{A}_2$ and $\mathbf{A}_3$).

We recall the coupled mode theory and transform it into the basis of instantaneous eigenstates to clearly see the evolution process. The simulated fields $\mathbf{A}(z)$ at different positions can be expanded as

$$\mathbf{A}(z) = a_2(z)\mathbf{A}_2(z) + a_1(z)\mathbf{A}_1(z) + a_3(z)\mathbf{A}_3(z), \tag{4}$$

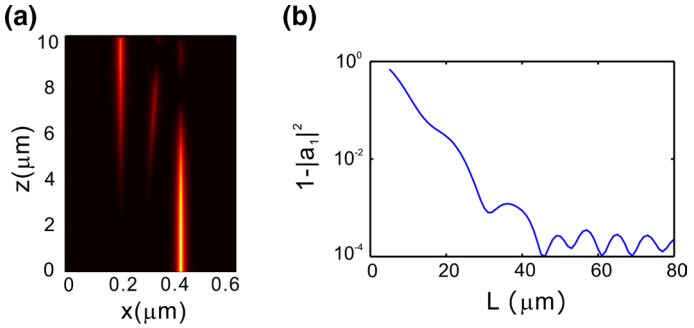

Fig. 3 The breakdown of adiabatic passage for a short propagation length. **a** The propagation of SPPs for $L = 10$ μm. **b** The probability of nonadiabatic energy transfer for different propagation lengths

where a_1, a_2, and a_3 represent the ratio of instantaneous eigenstates $\mathbf{A}_1(z)$, $\mathbf{A}_2(z)$, and $\mathbf{A}_3(z)$ to the total mode, respectively. The eigenstates are normalized by $\int|\mathbf{A}_{1,2,3}(x)|^2\mathrm{d}x=1$. The ratio a_j can be reconstructed from a solution $\mathbf{A}(z)$ via $a_j(z)=\int\mathbf{A}_j{}^*\mathbf{A}(z)\mathrm{d}x$ with $j=1, 2, 3$. We denote the ratio as $\mathbf{a}(z)=(a_2, a_1, a_3)^{\mathrm{T}}$. Then, Eq. (4) can be written as $\mathbf{A}(z)=\mathbf{R}(z)\mathbf{a}(z)$ with transfer matrix given by

$$\mathbf{R}=\frac{1}{\sqrt{2}}\begin{pmatrix}\sin\theta & \sqrt{2}\cos\theta & \sin\theta\\ 1 & 0 & -1\\ \cos\theta & -\sqrt{2}\sin\theta & \cos\theta\end{pmatrix}, \tag{5}$$

which is formed by the three normalized instantaneous eigenstates. Applying $\mathbf{A}(z)=\mathbf{R}(z)\mathbf{a}(z)$ into $-i\mathrm{d}\mathbf{A}/\mathrm{d}z=\mathbf{H}\mathbf{A}$, we arrive at the coupled mode theory in the basis of instantaneous eigenstates, that is,

$$-i\frac{d\mathbf{a}(z)}{dz}=\mathbf{H}^a(z)\mathbf{a}(z). \tag{6}$$

where $\mathbf{H}^{\mathrm{a}}=\mathbf{R}^{-1}\mathbf{H}\mathbf{R}+i\mathbf{R}^{-1}\mathrm{d}\mathbf{R}/\mathrm{d}z$. After simplification, we have

$$\mathbf{H}^a=\begin{pmatrix}\beta_0+\sqrt{c_1^2+c_2^2} & -i\frac{1}{\sqrt{2}}\frac{d\theta}{dz} & 0\\ i\frac{1}{\sqrt{2}}\frac{d\theta}{dz} & \beta_0 & i\frac{1}{\sqrt{2}}\frac{d\theta}{dz}\\ 0 & -i\frac{1}{\sqrt{2}}\frac{d\theta}{dz} & \beta_0-\sqrt{c_1^2+c_2^2}\end{pmatrix}. \tag{7}$$

The breakdown of adiabatic transfer can be easily understood from Eq. (7). As light is injected from right waveguide, the initial mode is equal to mode $\mathbf{A}_1$ and we have initial ratio as $\mathbf{a}(0)=(0, 1, 0)^{\mathrm{T}}$. Then $\mathbf{H}$a 1,2 and $\mathbf{H}$a 3,2 acts as nonadiabatic terms, which can couple mode $\mathbf{A}_1$ into other two modes $\mathbf{A}_2$ and $\mathbf{A}_3$. Therefore, the adiabatic energy transfer only holds for large propagation distance such that the value $-i/\sqrt{2}\mathrm{d}\theta/\mathrm{d}z$ is small enough. Figure 3b shows the simulated result of ratio of mode $\mathbf{A}_2$ and $\mathbf{A}_3$ as a function of propagation length. The ratio of nonadiabatic transition decreases as the propagation length increase. At $z=50$ μm, the nonadiabatic transfer ratio is relatively small, which reads as 0.03%.

3.2 Influence of loss

The optical loss of SPPs is remarkable and may hamper the practical application. Here, we investigate the influence loss on the adiabatic transfer of SPPs in the three-waveguide graphene couplers. We show a small decay can lead to a breakdown of adiabatic transfer, even when the propagation constants are only slightly modified.

We now investigate the influence of loss on the propagation constants when loss is present in different waveguides. The loss can be treated as pertubation for small values. When the left graphene sheet is lossy and the other two sheets are reguarded as lossless, the eigenvalues can be obtained by using the first-order perturbation method. They are given as $\beta_1=\beta_0+i\gamma\cos^2\theta$ and $\beta_{2,3}=\beta_0\pm(c2\ 1+c2\ 2)^{1/2}+i\gamma/2\sin^2\theta$, where γ is the imaginary part of propagation constants in single graphene sheet. The introduction of loss only results a small imaginary part of propagation constants while the real part remains

unchanged. The resulting eigenstates should be also perturbed compared to lossless case. The coupling strength relates to the interlayer spacing as $c_i = c_0 \exp(-\kappa d_i)$ with c_0 being constant and $\kappa = \mathrm{Re}(\beta_0 - \varepsilon_d k2\ 0)^{1/2}$ (Li et al. 2013; Golshani et al. 2014). The coupling coefficients can be extracted from the numerical values of propagation constants calculated by TMM. At $z = L/2$, we have $d_1 = d_2 = d/2$. Then, the constant c_0 can be figured out as $c_0 = [\beta_2(L/2) - \beta_3(L/2)]/[2\sqrt{2}\exp(-\kappa d/2)]$. The relaxation time of graphene now is chosen as $\tau = 1$ ps for the lossy graphene sheet. Then we have $\beta_0 = 43.4\ \mu\mathrm{m}^{-1}$, $\gamma = 0.34\ \mu\mathrm{m}^{-1}$, $\beta_2(L/2) = (42.92 + 0.08i)\ \mu\mathrm{m}^{-1}$ and $\beta_3(L/2) = (43.89 + 0.07i)\ \mu\mathrm{m}^{-1}$. Now we get $\kappa = 43.43\ \mu\mathrm{m}^{-1}$ and $c_0 = (40.7 - 0.46i)\ \mu\mathrm{m}^{-1}$. Figure 4a, b presents the propagation constants at different distances as the left graphene is lossy. The real part of propagation constants keeps unchanged with that all graphene is lossless. However, the propagation constants have imaginary part. The numerical results obtained by TMM method agree well with the theoretical indications.

When the middle graphene sheet is decayed, the eigenvalues can be directly calculated as $\beta_1 = \beta_0$ and $\beta_{2,3} = \beta_0 + i\gamma/2 \pm (c2\ 1 + c2\ 2 + \gamma^2/4)^{1/2}$. The coupling strength can be also extracted from the numerical results using the method discussed above. Figure 4b, c show propagation constants at different positions as the middle graphene is lossy. The real part of propagation constants keeps unchanged while the imaginary part is different. The propagation constants of dark mode (blue line and dots) are the same as the lossless case. When the right graphene sheet is decayed and the other two sheets are reguarded as lossless, the eigenvalues approximate as $\beta_1 = \beta_0 + i\gamma \sin^2\theta$ and $\beta_{2,3} = \beta_0 \pm (c2\ 1 + c2\ 2)^{1/2} + i\gamma/2\cos^2\theta$. Figure 4b, c show the propagation constants at different distances as the right graphene is lossy. The real part of propagation constants keeps unchanged while the imaginary part is different. For the dark mode, the initial propagation loss is relatively large at the beginning of the waveguide.

The above discussion implies small loss only slightly modifies the eigenvalues. However, the SPP propagations are quite different even if the decay is relatively small. Figure 5a–c show the propagation of SPPs as the left, middle, and right waveguides are decayed, respectively.

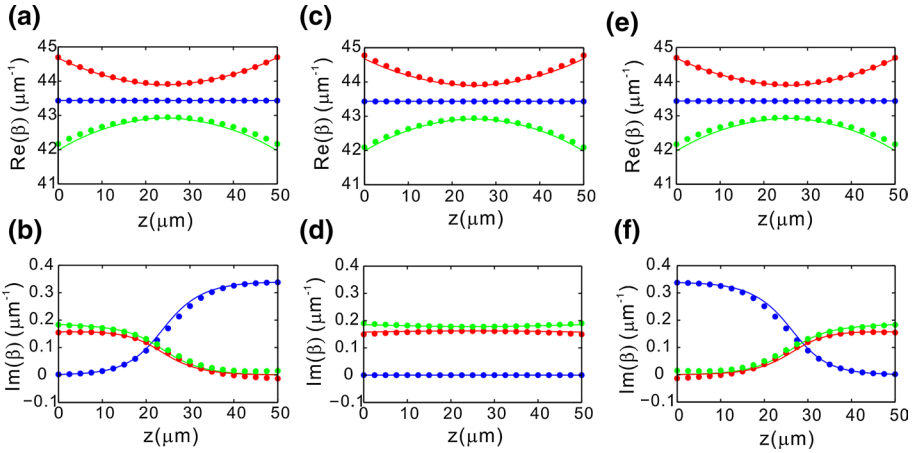

Fig. 4 The propagation constants as different waveguides are decayed. **a**, **b** The left waveguide is decayed. **c**, **d** The middle waveguide is decayed. **e**, **f** The right waveguide is decayed. **a**, **c**, and **e** plot the real part of propagation constants, while **b**, **d**, and **f** plot the imaginary part. The dots represent the results indicated by coupled mode theory and the lines are the numerical results. The different colors represent different modes. (Color figure online)

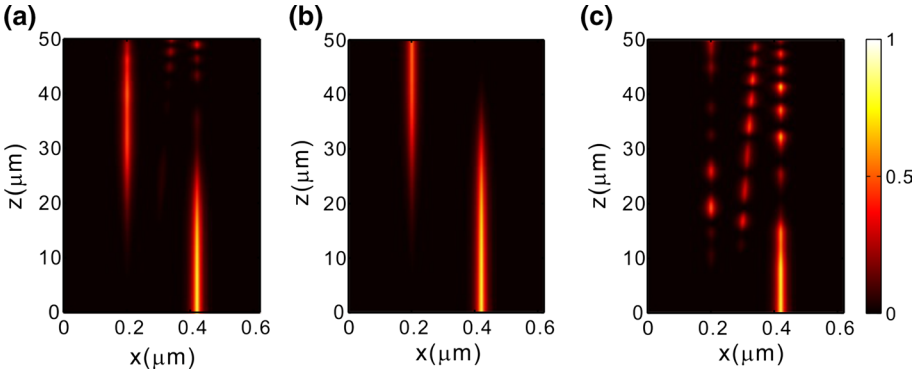

Fig. 5 The breakdown of adiabatic passage in present of loss. **a**–**c** correspond to the left, middle, and right waveguide is decayed, respectively. In all cases, the SPPs are launched from the right waveguide

The field intensity in Fig. 5c is normalized by the maximum at each position z to clearly see the field distribution at respect waveguide. The adiabatic transfer only holds when the middle waveguide is attenuated. This is because there is no energy residing at center waveguide for the dark mode and the decay of SPPs can be neglected. Therefore, the loss at center waveguide almost has no effect on the SPP propagation. However, when the left or the right waveguides are attenuated, the adiabatic transfer schemes break down and the three waveguides have energy at the output. The breakdown of adiabatic transfer may relate to two reasons. Firstly, the absolute value of nonadiabatic coupling may increase when loss is introduced. Secondly, the intensity of light decreases and the relative value of nonadiabatic coupling cannot be neglected.

When all the three waveguides are lossy, the wave propagation is also subject to Eq. (7) except that the propagation constants possess the additional small imaginary part. In this case, the nonadiabatic coupling **H**a 1,2 and **H**a 3,2 remain unchanged. Therefore, the adiabatic transfer can hold.

4 Restoration to adiabatic passage

The adiabatic energy transfer breaks down whether the propagation distance is not long enough or the loss is introduced in the left and the right waveguides. In the following, we show the nonadiabatic transfer can be suppressed by combining two cases when the gain and loss in respect waveguides are suitably designed.

We now investigate the coupled mode theory on the basis of eigenstates when the system is non-Hermitian. The transfer matrix is also assumed to be same as Eq. (5) by neglecting the influence of gain and loss on the eigenstates. The Hamiltonian **H** is taken account of the loss. When the left waveguide is decayed, the system Hamiltonian on the basis of eigenstates is given by

$$\mathbf{H}_a = \begin{pmatrix} \beta + \frac{i\gamma \sin\theta^2}{2} + \sqrt{c_1^2 + c_2^2} & i\frac{\gamma \sin 2\theta}{2\sqrt{2}} - i\frac{1}{\sqrt{2}}\frac{d\theta}{dz} & \frac{i\gamma \sin\theta^2}{2} \\ i\frac{\gamma \sin 2\theta}{2\sqrt{2}} + i\frac{1}{\sqrt{2}}\frac{d\theta}{dz} & \beta + i\gamma\cos\theta^2 & \frac{i\gamma \sin 2\theta}{2\sqrt{2}} + i\frac{1}{\sqrt{2}}\frac{d\theta}{dz} \\ \frac{i\gamma \sin\theta^2}{2} & i\frac{\gamma \sin 2\theta}{2\sqrt{2}} - i\frac{1}{\sqrt{2}}\frac{d\theta}{dz} & \beta + \frac{i\gamma \sin\theta^2}{2} - \sqrt{c_1^2 + c_2^2} \end{pmatrix}. \quad (8)$$

The terms **H**a (1,2) and **H**a (3,2) act as nonadiabatic coupling as the dark mode is initial excited, that is, $\mathbf{a}(0)=(0,\ 1,\ 0)^{\mathrm{T}}$. Therefore, the nonadiabatic coupling can be vanished by setting the terms

$$i\frac{\gamma \sin 2\theta}{2\sqrt{2}} - i\frac{1}{\sqrt{2}}\frac{d\theta}{dz} = 0 \tag{9}$$

As $\tan\theta = c_1/c_2$, the imaginary part of propagation constant should be $\gamma = \frac{d}{dz} Ln\frac{c_1}{c_2}$. Applying $c_i = c_0 \exp(-\kappa d_i)$ into the above equation, we can get $\gamma = -2\kappa(d-2d_0)/L$. This implies the left waveguide should be amplified and the absolute value of gain is constant at different positions. Figure 6a illustrates the wave propagation as the left waveguide is amplified for $L = 10$ μm. The imaginary part of propagation constant of left waveguide should be $\gamma = -0.52\ \mu\mathrm{m}^{-1}$. The corresponding surface conductivity of left waveguide is $\sigma_g = -9.2\times10^{-7} + 7.68\times10^{-5} i$ S. The result shows that the energy gradually transfers into the right waveguide. Only a small amount of energy turns into center waveguide at the initial propagation. The SPPs dominates at the left waveguide while the other two waveguides are almost dark. Therefore, the nonadiabatic transfer can be vanished. Now the propagation distance is also reduced.

When the right waveguide is decayed, the system Hamiltonian reads as

$$\mathbf{H}_a = \begin{pmatrix} \beta_0 + \frac{i\gamma\cos^2\theta}{2} + \sqrt{c_1^2 + c_2^2} & -\frac{i\gamma\sin 2\theta}{2\sqrt{2}} - \frac{i}{\sqrt{2}}\frac{d\theta}{dz} & \frac{i\gamma\cos^2\theta}{2} \\ -\frac{i\gamma\sin 2\theta}{2\sqrt{2}} + \frac{i}{\sqrt{2}}\frac{d\theta}{dz} & \beta_0 + i\gamma\sin^2\theta & -\frac{i\gamma\sin 2\theta}{2\sqrt{2}} + \frac{i}{\sqrt{2}}\frac{d\theta}{dz} \\ \frac{i\gamma\cos^2\theta}{2} & -\frac{i\gamma\sin 2\theta}{2\sqrt{2}} - \frac{i}{\sqrt{2}}\frac{d\theta}{dz} & \beta_0 + \frac{i\gamma\cos^2\theta}{2} - \sqrt{c_1^2 + c_2^2} \end{pmatrix} \tag{10}$$

Similarly, the nonadiabatic terms are vanished when $\gamma = 2\kappa(d-2d_0)/L$, which implies one should add loss into right waveguide. The amount of loss is related to propagation distance L. For the parameter we choose, the imaginary part of propagation constants should be $\gamma = 0.52\ \mu\mathrm{m}^{-1}$ as $L = 10$ μm. The relaxation time of lossy graphene should be $\tau = 0.65$ ps. Figure 6b presents the propagation of SPPs as the right waveguide is decayed

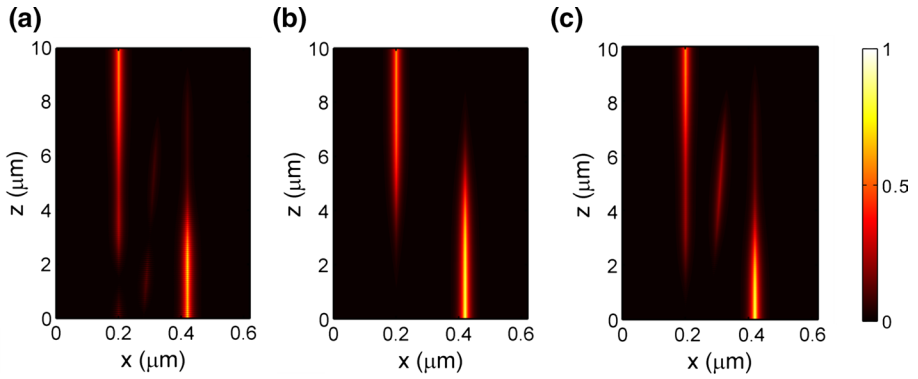

Fig. 6 The restoration of adiabatic passage by adding certain gain and loss in respect waveguides. **a** The left waveguide is with gain. **b** The right waveguide is with loss. **c** The left waveguide is with gain and the right waveguide is with the same amount of loss. The transverse field distribution is normalized by the total energy at each position z

for $L=10$ μm. The SPPs transfer into the left waveguide as middle waveguide remains dark during the propagation. Moreover, the propagation distance is effectively decreased when compared with that shown in Fig. 2c.

Another case is to add balanced gain and loss in left and right waveguides simultaneously. The system Hamiltonian can be given by

$$\mathbf{H}_a = \begin{pmatrix} \beta_0 + \frac{i\gamma\cos^2\theta}{2} + \sqrt{c_1^2+c_2^2} & -\frac{i\gamma\sin 2\theta}{2\sqrt{2}} - \frac{i}{\sqrt{2}}\frac{d\theta}{dz} & -\frac{i\gamma\sin^2\theta}{2} - \frac{i\gamma}{2} \\ -\frac{i\gamma\sin 2\theta}{2\sqrt{2}} + \frac{i}{\sqrt{2}}\frac{d\theta}{dz} & \beta_0 - i\gamma\cos^2\theta & -\frac{i\gamma\sin 2\theta}{2\sqrt{2}} + \frac{i}{\sqrt{2}}\frac{d\theta}{dz} \\ -\frac{i\gamma\sin^2\theta}{2} - \frac{i\gamma}{2} & -\frac{i\gamma\sin 2\theta}{2\sqrt{2}} - \frac{i}{\sqrt{2}}\frac{d\theta}{dz} & \beta_0 + \frac{i\gamma\cos^2\theta}{2} - \sqrt{c_1^2+c_2^2} \end{pmatrix} \tag{11}$$

The condition to offset the nonadiabatic term is the same as that in Fig. 6b. The gain and loss coefficient is given by $\gamma=2\kappa(d-2d_0)/L$. The corresponding surface conductivity of left and right waveguides is $\sigma_g=\mp 9.2\times10^{-7}+7.68\times10^{-5}i$ S, respectively. Figure 6c illustrate the wave propagation as the left and right waveguides are with balanced gain and loss for $L=10$ μm. One can see the energy gradually transfer into the right waveguide. Only a small amount of energy translates into the center waveguide during the initial propagation.

In experiment, the gain in graphene is not easily realized. The most possible way to observe the predicted phenomenon is to use passive graphene waveguides, in which the waveguide with lower loss acts as the amplified waveguide. The results in passive waveguides should be similar to that in the waveguides with gain and loss. The loss of graphene relates to relaxation time τ, which can be directly controlled by varying the chemical potential via electrostatic and chemical doping. When changing the surrounding environment such as placing organic molecules on graphene, the carrier mobility will be significantly enhanced, leading to the increasing of relaxation time. So the loss of graphene can be tuned by controlling environment and chemical potential (Wang et al. 2010).

5 Conclusion

In conclusion, we have demonstrated the energy transfer of SPPs based on STIRAP in a three-waveguide graphene coupler. The SPPs can effectively transfer between two outer waveguides while the center waveguide remains dark, provided that waveguides are lossless and the propagation distance is long enough. We show the small loss of graphene can lead to a breakdown of adiabatic transfer schemes, even when the wavevector of three-waveguide graphene coupler is only slightly modified. By analyzing the coupled mode theory on the basis of eigenmodes, we propose three approaches to cancel the nonadiabatic coupling, which is done by adding constant gain or loss in respect waveguides. Through these approaches, the coupling length of the waveguide is effectively decreased. The study may find interesting application in optical switches on a deep-subwavelength scale by taking advantage of the non-Hermitivity present in the system.

Acknowledgements Program for Distinguished Middle-aged and Young Innovative Research Team in Higher Education of Hubei, China (T201806), the Campus Science Foundation Research Project of Wuhan Institute of Technology (K201821).

References

Bao, Q., Loh, K.P.: Graphene photonics, plasmonics, and broadband optoelectronic devices. ACS Nano **6**(5), 3677–3694 (2012)

Boubanga-Tombet, S., Chan, S., Watanabe, T., Satou, A., Ryzhii, V., Otsuji, T.: Ultrafast carrier dynamics and terahertz emission in optically pumped graphene at room temperature. Phys. Rev. B **85**(3), 035443 (2012)

Chen, P.Y., Jung, J.: PT symmetry and singularity-enhanced sensing based on photoexcited graphene metasurfaces. Phys. Rev. Appl. **5**(6), 064018 (2016)

Chen, Y., Zhou, Y., Li, Y., Li, M., Lan, P., Lu, P.: Rabi oscillation in few-photon double ionization through doubly excited states. Phys. Rev. A **97**(1), 013428 (2018)

De Leon, I., Berini, P.: Amplification of long-range surface plasmons by a dipolar gain medium. Nat. Photon. **4**(6), 382–387 (2010)

Deng, H., Ye, F., Malomed, B.A., Chen, X., Panoiu, N.C.: Optically and electrically tunable Dirac points and Zitterbewegung in graphene-based photonic superlattices. Phys. Rev. B **91**, 201402(R) (2015)

Deng, H., Chen, X., Malomed, B.A., Panoiu, N.C., Ye, F.: Tunability and robustness of Dirac points of photonic nanostructures. IEEE J. Sel. Top. Quant. Electron. **22**(5), 5000509 (2016)

Dreisow, F., Ornigotti, M., Szameit, A., Heinrich, M., Keil, R., Nolte, S., Tünnermann, A., Longhi, S.: Polychromatic beam splitting by fractional stimulated Raman adiabatic passage. App. Phys. Lett. **95**(26), 261102 (2009)

Gan, F., Sun, C., Wang, Y., Li, H., Gong, Q., Chen, J.: Multimode metallic double-strip waveguides for polarization manipulation. Adv. Mater. Technol. **2**(4), 1600248 (2017)

Golshani, M., Weimann, S., Jafari, K., Khazaei Nezhad, M., Langari, A., Bahrampour, A.R., Eichelkraut, T., Mahdavi, S.M., Szameit, A.: Impact of loss on the wave dynamics in photonic waveguide lattices. Phys. Rev. Lett. **113**, 123903 (2014)

Graefe, E., Mailybaev, A.A., Moiseyev, N.: Breakdown of adiabatic transfer of light in waveguides in the presence of absorption. Phys. Rev. A **88**, 033842 (2013)

Gramotnev, D.K., Bozhevolnyi, S.I.: Plasmonics beyond the diffraction limit. Nat. Photon. **4**(2), 83–91 (2010)

He, M., Zhou, Y., Li, Y., Li, M., Lu, P.: Revealing the target structure information encoded in strong-field photoelectron hologram. Opt. Quant. Electron. **49**(6), 232 (2017)

He, L., Zhang, Q., Lan, P., Cao, W., Zhu, X., Zhai, C., Wang, F., Shi, W., Li, M., Bian, X., Lu, P., Bandrauk, A.D.: Monitoring ultrafast vibrational dynamics of isotopic molecules with frequency modulation of high-order harmonics. Nat. Commun. **9**, 1108 (2018a)

He, M., Li, Y., Zhou, Y., Li, M., Cao, W., Lu, P.: Direct visualization of valence electron motion using strong-field photoelectron holography. Phys. Rev. Lett. **120**(13), 133204 (2018b)

He, L., Lan, P., Le, A.T., Wang, B., Wang, B., Zhu, X., Lu, P., Lin, C.D.: Real-time observation of molecular spinning with angular high-harmonic spectroscopy. Phys. Rev. Lett. **121**, 163201 (2018c)

Hong, Z., Rezvani, S., Zhang, Q.: Octave-spanning energy-scalable CEP-stabilized pulses from a dual-chirped noncollinear optical parametric amplifier. Opt. Quant. Electron. **49**, 392 (2017)

Hong, Z., Zhang, Q., Ali Rezvani, S., Lan, P., Lu, P.: Tunable few-cycle pulses from a dual-chirped optical parametric amplifier pumped by broadband laser. Opt. Laser Technol. **98**, 169–177 (2018)

Huang, Z., Wang, L., Sun, B., He, M., Liu, J., Li, H., Zhai, X.: A mid-infrared fast-tunable graphene ring resonator based on guided-plasmonic wave resonance on a curved graphene surface. J. Opt. **16**(105004), 1–7 (2014)

Huang, H., Ke, S., Wang, B., Long, H., Wang, K., Lu, P.: Numerical study on plasmonic absorption enhancement by a rippled graphene sheet. J. Lightwave Technol. **35**(2), 320–324 (2017)

Ibáñez, S., Muga, J.G.: Adiabaticity condition for non-Hermitian Hamiltonians. Phys. Rev. A **89**(3), 033403 (2014)

Ke, S., Wang, B., Qin, C., Long, H., Wang, K., Lu, P.: Exceptional points and asymmetric mode switching in plasmonic waveguides. J. Lightwave Technol. **34**(22), 5258–5262 (2016)

Ke, S., Wang, B., Long, H., Wang, K., Lu, P.: Topological mode switching in a graphene doublet with exceptional points. Opt. Quant. Electron. **49**, 224 (2017)

Ke, S., Zhao, D., Liu, Q., Wu, S., Wang, B., Lu, P.: Optical imaginary directional couplers. J. Lightwave Technol. **36**(12), 2510–2516 (2018a)

Ke, S., Liu, J., Liu, Q., Zhao, D., Liu, W.: Strong absorption near exceptional points in plasmonic waveguide arrays. Opt. Quant. Electron. **50**, 318 (2018b)

Ke, S., Liu, Q., Zhao, D., Liu, W.: Spectral discrete diffraction with non-Hermitian coupling. J. Opt. Soc. Am. B **35**(10), 2387 (2018c)

Konstantatos, G., Badioli, M., Gaudreau, L., Osmond, J., Bernechea, M.: Hybrid graphene-quantum dot phototransistors with ultrahigh gain. Nat. Nanotechnol. **7**(6), 363–368 (2012)

Kou, Y., Ye, F., Chen, X.: Multiband Vector Plasmonic Lattice Solitons. Opt. Lett. **38**(8), 1271–1273 (2013)

Lan, P., Ruhmann, M., He, L., Zhai, C., Wang, F., Zhu, X., Zhang, Q., Zhou, Y., Li, M., Lein, M., Lu, P.: Attosecond probing of nuclear dynamics with trajectory-resolved high-harmonic spectroscopy. Phys. Rev. Lett. **119**(3), 033201 (2017)

Li, T., Luo, L., Hupalo, M., Zhang, J., Tringides, M.C., Schmalian, J., Wang, J.: Femtosecond population inversion and stimulated emission of dense Dirac fermions in graphene. Phys. Rev. Lett. **108**(16), 167401 (2012)

Li, Y., Guo, X., Xu, C., Yang, J., Jiang, X., Wang, M.: Coupled mode theory under the parity-time symmetry frame. J. Lightwave Technol. **31**(15), 2477–2481 (2013)

Li, G., Chen, G., Peng, P., Qi, W.: Non-Hermitian shortcut to adiabaticity of two- and three-level systems with gain and loss. Eur. Phys. J. D **71**(14), 1–10 (2017)

Li, L., Lan, P., He, L., Zhu, X., Chen, J., Lu, P.: Scaling Law of High Harmonic Generation in the Framework of Photon Channels. Phys. Rev. Lett. **120**(22), 223203 (2018)

Lin, X., Li, R., Gao, F., Li, E., Zhang, X., Zhang, B., Chen, H.: Loss induced amplification of graphene plasmons. Opt. Lett. **41**(4), 681–684 (2016a)

Lin, X., Rivera, N., López, J.J., Kaminer, I., Chen, H., Soljačić, M.: Tailoring the energy distribution and loss of 2D plasmons. New J. Phys. **18**(10), 105007 (2016b)

Liu, Q., Ke, S., Liu, W.: Mode conversion and absorption in an optical waveguide under cascaded complex modulations. Opt. and Quant. Electron. **50**, 356 (2018a)

Liu, W., Li, X., Song, Y., Zhang, C., Han, X., Long, H., Wang, B., Wang, K., Lu, P.: Cooperative enhancement of two-photon-absorption-induced photoluminescence from a 2D perovskite-microsphere hybrid dielectric structure. Adv. Funct. Mater. **28**(26), 1707550 (2018b)

Liu, K., Qin, M., Li, Q., Liao, Q.: Transition from strong-field sequential to nonsequential double ionization at near-infrared wavelengths and low intensities. Opt. Quantum. Electron. **50**(10), 364 (2018c)

Ma, X., Zhou, Y., Li, N., Li, M., Lu, P.: Attosecond control of correlated electron dynamics in strong-field nonsequential double ionization by parallel two-color pulses. Opt. Laser Technol. **108**, 235–240 (2018)

Makris, K.G., El-Ganainy, R., Christodoulides, D.N.: Beam dynamics in PT symmetric optical lattices. Phys. Rev. Lett. **100**, 103904 (2008)

Milburn, T.J., Doppler, J., Holmes, C.A., Portolan, S., Rotter, S., Rabl, P.: General description of quasiadiabatic dynamical phenomena near exceptional points. Phys. Rev. A **92**(5), 052124 (2015)

Mrejen, M., Suchowski, H., Hatakeyama, T., Wu, C., Feng, L., O'Brien, K., Wang, Y., Zhang, X.: Adiabatic elimination-based coupling control in densely packed subwavelength waveguides. Nat. Commun. **6**, 7565 (2015)

Ni, G.X., Wang, L., Goldflam, M.D., Wagner, M., Fe, Z., McLeo, A.S., Liu, M.K., Keilman, F., Özyilmaz, B., Castro Neto, A.H., Hone, J., Fogler, M.M., Basov, D.N.: Ultrafast optical switching of infrared plasmon polaritons in high-mobility graphene. Nat. Photon. **10**, 244–247 (2016)

Paspalakis, E.: Adiabatic three-waveguide directional coupler. Opt. Commun. **258**, 30–34 (2006)

Qin, C., Wang, B., Long, H., Wang, K., Lu, P.: Nonreciprocal phase shift and mode modulation in dynamic graphene waveguides. J. Lightwave Technol. **34**(16), 3877–3883 (2016)

Qin, C., Zhou, F., Peng, Y., Sounas, D., Zhu, X., Wang, B., Dong, J., Zhang, X., Alù, A., Lu, P.: Spectrum control through discrete frequency diffraction in the presence of photonic gauge potentials. Phys. Rev. Lett. **120**, 133901 (2018)

Ryzhii, V., Ryzhii, M., Mitin, V., Otsuji, T.: Toward the creation of terahertz graphene injection laser. J. Appl. Phys. **110**(9), 094503 (2011)

Sharaf, R., Dehghani, M., Ramezani, H.: Effect of non-Hermiticity on adiabatic elimination in coupled waveguides. Phys. Rev. A **97**, 013854 (2018)

Sounas, D.L., Alù, A.: Non-reciprocal photonics based on time modulation. Nat. Photonics **11**, 774–783 (2017)

Sun, C., Rong, K., Wang, Y., Li, H., Gong, Q., Chen, J.: Plasmonic ridge waveguides with deep-subwavelength outside-field confinements. Nanotechnology **27**(6), 065501 (2016)

Tan, J., Li, Y., Zhou, Y., He, M., Chen, Y., Li, M., Lu, P.: Identifying the contributions of multiple-returning recollision orbits in strong-field above-threshold ionization. Opt. Quant. Electron. **50**(2), 57 (2018)

Torosov, B.T., Valle, G.D., Longhi, S.: Non-Hermitian shortcut to stimulated Raman adiabatic passage. Phys. Rev. A **89**, 063412 (2014)

Vitanov, N.V., Rangelov, A.A., Shore, B.W., Bergmann, K.: Stimulated Raman adiabatic passage in physics, chemistry, and beyond. Rev. Mod. Phys. **89**, 015006 (2017)

Wang, D., Liu, X., He, L., Yin, Y., Wu, D., Shi, J.: Manipulating graphene mobility and charge neutral point with ligand-bound nanoparticles as charge reservoir. Nano Lett. **10**(12), 4989–4993 (2010)
Wang, F., Qin, C.Z., Wang, B., Long, H., Wang, K., Lu, P.X.: Rabi oscillations of plasmonic supermodes in graphene multilayer arrays. IEEE J. Sel. Top. Quant. **23**(1), 4600105 (2017a)
Wang, S., Wang, B., Qin, C., Wang, K., Long, H., Lu, P.: Rabi oscillations of optical modes in a waveguide with dynamic modulation. Opt. Quant. Electron. **49**, 389 (2017b)
Wang, Z., Wang, B., Long, H., Wang, K., Lu, P.: Surface plasmonic lattice solitons in semi-infinite graphene sheet arrays. J. Lightwave Technol. **35**(14), 2960–2965 (2017c)
Wang, F., Ke, S., Qin, C., Wang, B., Long, H., Wang, K., Lu, P.: Topological interface modes in graphene multilayer arrays. Opt. Laser Technol. **103**, 272–278 (2018a)
Wang, B., He, L., Wang, F., Yuan, H., Zhu, X., Lan, P., Lu, P.: Resonance-modulated wavelength scaling of high-order-harmonic generation from. Phys. Rev. A **97**(1), 013417 (2018b)
Wu, Q., Chen, Y., Huang, B., Song, J., Xia, Y., Zheng, S.-B.: Improving the stimulated Raman adiabatic passage via dissipative quantum dynamics. Opt. Express **24**(20), 22847–22864 (2016)
Yuan, H., He, L., Wang, F., Wang, B., Liu, W., Hong, Z.: Generation of isolated attosecond pulses in a multi-cycle inhomogeneous two-color field without CEP stabilization. Opt. Quant. Electron. **49**(6), 214 (2017)
Yuan, H., He, L., Wang, F., Wang, B., Zhu, X., Lan, P., Lu, P.: Tomography of asymmetric molecular orbitals with a one-color inhomogeneous field. Opt. Lett. **43**(4), 931 (2018)
Zhao, D., Wang, Z., Long, H., Wang, K., Wang, B., Lu, P.: Optical bistability in defective photonic multilayers doped by graphene. Opt. Quant. Electron. **49**, 163 (2017)
Zhao, D., Liu, W., Ke, S., Liu, Q.: Large lateral shift in complex dielectric multilayers with nearly parity-time symmetry. Opt. Quant. Electron. **50**, 323 (2018)